

Research Article

Differences in Nanosecond Laser Ablation and Deposition of Tungsten, Boron, and WB_2/B Composite due to Optical Properties

Tomasz Moscicki

Institute of Fundamental Technological Research, PAS, Pawinskiego 5B, 02-106 Warsaw, Poland

Correspondence should be addressed to Tomasz Moscicki; tmosc@ippt.pan.pl

Received 26 November 2015; Revised 24 March 2016; Accepted 18 April 2016

Academic Editor: Giulio Cerullo

Copyright © 2016 Tomasz Moscicki. This is an open access article distributed under the Creative Commons Attribution License, which permits unrestricted use, distribution, and reproduction in any medium, provided the original work is properly cited.

The first attempt to the deposition of WB_3 films using nanosecond Nd:YAG laser demonstrated that deposited coatings are superhard. However, they have very high roughness. The deposited films consisted mainly of droplets. Therefore, in the present work, the explanation of this phenomenon is conducted. The interaction of Nd:YAG nanosecond laser pulse with tungsten, boron, and WB_2/B target during ablation is investigated. The studies show the fundamental differences in ablation of those materials. The ablation of tungsten is thermal and occurs due to only evaporation. In the same conditions, during ablation of boron, the phase explosion and/or fragmentation due to recoil pressure is observed. The deposited films have a significant contribution of big debris with irregular shape. In the case of WB_2/B composite, ablation is significantly different. The ablation seems to be the detonation in the liquid phase. The deposition mechanism is related mainly to the mechanical transport of the target material in the form of droplets, while the gaseous phase plays marginal role. The main origin of differences is optical properties of studied materials. A method estimating phase explosion occurrence based on material data such as critical temperature, thermal diffusivity, and optical properties is shown. Moreover, the effect of laser wavelength on the ablation process and the quality of the deposited films is discussed.

1. Introduction

In recent years, growing interest in ultraincompressible and superhard materials has been observed. Tungsten triboride WB_3 is one of the most promising inexpensive candidates for ultraincompressible, superhard materials [1, 2]. Even in the form of thin films, it has superhard properties [3, 4] and, in the future, may be an alternative to other hard coatings, such as diamond-like DLC or cubic boron nitride (c-BN). One of the most promising methods of obtaining WB_3 films is pulsed laser deposition (PLD), because it highly suits deposition of hardly meltable metals, such as tungsten [5]. Pulsed laser deposition is a technique where a pulsed laser beam is focused inside a vacuum chamber to strike a target of the material that is to be deposited. This material is ablated from the target, forms a plasma plume, and subsequently deposits as a thin film on a substrate. Deposited films may have a thickness from several nanometres to several micrometres. The deposition of high-quality films requires knowledge of the first step

of the pulsed laser deposition process, which is laser ablation. The course of target ablation affects plasma plume composition, for example, vapour to nanoparticle and microparticle ratio.

The exact structure of tungsten borides is still a matter of vigorous debate in the literature. Recently, it has been found that the previously experimentally attributed WB_4 is in fact the defect-containing WB_3 [2, 5]. The first attempt to the deposition of WB_3 films using nanosecond Nd:YAG laser demonstrated that deposited coatings are superhard; however, they have very high roughness [5]. Additionally, the deposited debris has regular circular shape like droplets. The mechanism of deposition of droplets on the substrate surface may be explained by the condensation in plasma plume [6, 7]. Ablation plumes induced by nanosecond laser irradiation provide conditions which are well suited to the formation of nanoclusters. The high saturation ratios and presence of ionization lead to extraordinarily high nucleation rates and small

critical radii. In the case of condensation, only clusters in the range of 5–50 nm can be produced [6–8], which is above one hundred times less than dimension of droplets deposited in WB_3 films [5]. Moreover, the SEM-EDS study has shown that the composition of deposited film is close to the target one. It is impossible to get such results by the condensation only. All these phenomena indicate that film is deposited mainly from droplets erupted from target. This is a characteristic process of the ablation of very porous targets [9]. However, in this case, the porosity of target was negligible [5].

The simple mechanism of ablation consists of three stages. During the interaction of the laser beam with a material, the target is heated to a temperature exceeding its boiling point and sometimes also its critical temperature. In the second stage, material evaporated from the target forms a thin layer of dense plume, consisting of electrons, ions, and neutrals. This plasma plume absorbs energy from the laser beam (by means of photoionization and inverse Bremsstrahlung) and its temperature and pressure grow. The resulting pressure gradient accelerates the plume to high velocity perpendicular to the target. At the next time steps, the laser pulse terminates and plasma plume expands adiabatically [10, 11]. However, a considerable fraction of the plasma energy is reemitted and coupled back to the target and also affect the dynamics of plasma plume [12]. This ablation pattern can be used up to some limit of fluence in which there is no phase explosion yet [11, 13]. It is assumed that the explosive boiling begins when the temperature exceeds 0.9 of the critical temperature [11]. This type of ablation results in the appearance of nano- and microparticles in the plasma plume. The size and shape of deposited debris depend on material properties and time step during ablation process. The subsurface overheating during laser pulse and subsequent eruption [13] causes deposition of a mixture of vapours, irregular debris, and droplets. After the cessation of laser impulse, the thermal diffusion and subsequent explosive boiling are a potential mechanism. The superheated liquid will undergo a transition into a mixture of vapour and liquid droplets, followed by delayed explosive boiling of the liquid-vapour mix [14, 15]. Lu et al. demonstrated that in the case of ablation of single-crystal silicon and power density 2×10^{10} W/cm², large (micron-sized) droplets are ejected from the target after 300–400 ns of impulse cessation [14]. During deposition WB_3 from WB_2/B , the power density was about 10^9 W/cm² [5]. According to the presented theory [14], such power density is not sufficient to obtain droplets having a diameter of several micrometres. Therefore, the reasons for, as presented in [5], PLD process must be in the course of ablation of individual components of the SPS sintered WB_2/B target.

Besides the deposition of functional films containing boron [3, 16] or tungsten [4], the laser ablation is also used in applications such as micromachining [17], cleaning [18], and also fabrication of micro/nanostructures [19]. Tungsten is one of very few possible materials for in-vessel components in forward looking thermonuclear reactors. Therefore, any investigation of its properties and behaviour is very important, and in particular the characterisation of its evaporation processes from the inner wall of a tokamak chamber is needed [20].

Despite of numerous applications, the physics of laser ablation process is not yet thoroughly understood. It depends on not only the properties of the material but also laser parameters such as pulse duration, frequency [17], fluence [13], and wavelength [21].

Therefore, detailed knowledge on laser-induced flow dynamics of plasma and understanding of the mechanisms of ablation is necessary for optimizing technological processes of deposition of new materials and promoting powerful lasers with nanosecond pulse durations for cost-effective use in industries.

The main goal of this paper is the comparative analysis of boron, tungsten, and WB_2/B composite ablation processes induced by nanosecond laser radiation in vacuum. The unusual mechanism of ablation of WB_2/B target and deposition of WB_3 films are explained. Moreover, the effect of laser wavelength on the ablation process and the quality of the deposited boron and tungsten films is discussed.

2. Material and Experimental Methods

Irradiation of a tungsten and boron targets was performed using a Nd:YAG laser (Quantel, 981 E) in a chamber evacuated to a residual pressure of 1×10^{-5} Pa. The laser beam (10 ns FWHM) was focused to a spot size of 0.055 mm^2 with a fluence of 10 J/cm^2 . The distance from target to substrate was 4 cm. Thin films were deposited on a silicon (100) polished substrates (SPI Supplies) in ambient temperature. During deposition, the target was rotated to avoid crater formation. The deposition time was 30 minutes (18000 pulses) for each experiment. All ablation parameters were the same as in theoretical model. Both harmonics were polarized horizontally. The spatial and time profiles of the laser beam were Gaussian. The surface area of a laser spot was determined by registration of the spot size by ICCD camera after attenuation of the laser beam and was 0.075 mm^2 in the case of 1064 nm and 0.053 mm^2 in the case of 355 nm wavelength. The incident angle of the laser beam was 45° to the surface normal. The diameter of the laser spot used for calculations is equal to the average value of the ellipse diameters. The high-quality targets, boron from Kurt J. Lesker (2.35 g/cm^3 mass density, 99.5% purity) and tungsten from Kurt J. Lesker (19.35 g/cm^3 , 99.95% purity), were used. WB_2/B targets were fabricated from boron (~625 mesh, 99.7% purity, Sigma Aldrich) and tungsten ($12 \mu\text{m}$, 99.9% purity, Sigma Aldrich). Both elements were milled and mixed in the molar ratio 4.5:1 [3, 5]. The WB_2/B target was made in the spark plasma sintering process (SPS). Mersen (Carbone Lorraine) tools were placed in the sintering chamber of the furnace HP D 25-3. Sintering process was conducted in vacuum at a sintering temperature of 1600°C , and under a compaction pressure of 50 MPa. The heating rate was 50°C/min and the sintering time was 2.5 min. The duration of a single current impulse was equal to 15 ms, and the interval between the impulses lasted 3 ms. Cylindrical samples with diameter of 20 mm were produced.

The laser deposited films surface was subject to inspection under a Scanning Electron Microscope: JEOL, JSM-6010PLUS/LV InTouchScope™. In addition, the EDS micro-analysis was used to study the elemental distribution of

boron and tungsten in the targets and deposited films. The crater shape after 50 impulses was measured with Confocal Microscope: Keyence V \times 100. The images of the plasma plume were registered with the use of an ICCD camera. The plasma was imaged on the camera using a 180 cm focal length camera lens. The image intensifier was gated for an exposure time of 5 ns, while the delay time between the laser pulse and the pulse triggering the image intensifier was changed gradually.

3. Theory/Calculation

The theoretical model, that describes the target heating, formation of the plasma, and its expansion, was previously presented in [22, 23]. The main goal of the present research is a comparative analysis of ablation mechanism of WB₂/B, boron, and tungsten target and the impact of this phenomenon on the composition of the plasma for different laser wavelengths. It should be emphasized that the absorption of the laser beam depends mainly on the optical properties of the material such as depth of penetration and reflectivity. Calculations were made for two wavelengths of an Nd:YAG laser: 355 nm and 1064 nm. The laser beam with a Gaussian profile (10 ns FWHM) was focused to a spot size of 0.055 mm² with a fluence of 10 J/cm². It was assumed that the boron or tungsten plume expands to ambient air at a pressure of 10⁻³ Pa.

The intensity of laser beam reaching the target surface I_L was used in the form which fits the shape of the laser pulse used in our experiments:

$$I_L(t, r) = \frac{CF}{\tau} \exp\left(-\left(\frac{t-t_0}{s_2}\right)^2\right) \exp\left(-\left(\frac{r}{s_1}\right)^2\right) \cdot \left(\exp\left(-\int \kappa dz\right)\right), \quad (1)$$

where $s_1 = 0.098 \times 10^{-3}$ m and $s_2 = 6.0056 \times 10^{-9}$ s are Gauss parameters, F is the laser fluence, τ is the laser pulse duration, κ is the plasma absorption coefficient, r and z are radial and axial coordinate, respectively, and the integration is over the distance travelled by the beam. The numerical factor C results from normalization; t_0 is the time offset of the beam maximum intensity. The first part of (1) describes temporal evolution of the laser intensity and the second energy distribution in the laser beam and the last exponential component takes into account the attenuation of the laser beam on its way to the point (r, z) in plasma. The 45° incidence angle was taken into account by the multiplying of laser beam way by factor $\sqrt{2}$.

The laser radiation reflected from the surface of target R was included. Due to reflectance, the source component in energy equation is $\kappa I_L(1 + R)$ in the case of plasma and $\alpha I_L(1 - R)\exp(-\int \alpha dz_T)$ for the target. The exponential component takes into account the attenuation of the laser beam on its way to the point (r, z_T) of target. Because, during pulse termination, plasma plume has small dimension and is connected with target, the change of laser beam incidence angle from normal to 45 degrees does not reduce absorption

of energy from laser beam. Oppositely, the extended way (by factor $\sqrt{2}$) increases absorbed energy.

The used ablation model consists of two parts. The first part, which is settled with conduction equation with energy source due to laser irradiation [22, 24], was responsible for the determination of the temperature distribution and mass removal in the target. In the second part, the Eulerian system of equations of continuity and the diffusion equation [22, 24] were solved for plasma.

The system of equations was solved iteratively. The target temperature was calculated and then the stream of ablated particles was determined at the end of the Knudsen layer. These conditions were taken as inlet conditions for plume expansion. Next, the absorption of the laser radiation in developing the plasma plume was determined and the target temperature was recalculated according to actual laser intensity at the target surface. The new target temperature was used to determine the conditions at the end of the Knudsen layer, which were subsequently used as inlet conditions for plume expansion. The other boundary conditions for plasma system of equations were as follows. The stream of boron or tungsten vapour was directed perpendicularly to the target surface. At the wall, the noslip boundary and a fixed temperature condition were applied. At the outflow boundary, the pressure outlet boundary conditions [24] were used, which required the specification of a static pressure at the outlet boundary. This static pressure value is relative to the operating pressure. The axis boundary conditions were used at the centerline of the axisymmetric geometry [24].

The boundary condition at the place where the laser beam strikes the surface of target is

$$-k \frac{\partial T_s}{\partial \vec{n}} = -\rho \vec{u}(t) L_v + \frac{\varepsilon}{2}, \quad (2)$$

where \vec{u} is the recession velocity given by the Hertz-Knudsen equation [13, 25], L_v is the latent heat of vaporization, and \vec{n} is the unit vector perpendicular to the surface. The last part of (2) describes target heating due to plasma radiation ε . Energy losses due to thermal radiation from the surface of target are small compared to other terms and were neglected.

All the material functions of tungsten and boron were described in [22] and depend on the temperature, pressure, and mass fraction. WB₂ target properties also depend on temperature and were as follows: heat capacity at room temperature $c_p = 308$ J/kgK and at melting point $c_p = 364$ J/kgK [26], thermal conductivity at room temperature $k = 43$ W/mK and at melting point $k = 32$ W/mK [27], density $\rho = 12890$ kg/m³ [26], and the melting temperature $T_m = 2833$ K [26]. Because there is lack of data about boiling point of WB₂, ZrB₂ data was adopted; that is, boiling temperature $T_b = 2400$ K under background pressure $p_b = 2 \times 10^{-3}$ Pa and latent heat of vaporization $L_v = 466.9 \pm 6.5$ kcal/mol [28]. Bolgar et al. [29] determined the vapour pressures and heats of vaporization of fourteen refractory compounds among which were TiB₂, ZrB₂, CrB₂, and AlB₁₂. Latent heat of vaporization all of these borides does not differ more than 20%. Because WB₂ also belongs to the group of refractory borides, the assumption about its boiling point parameters appears to be correct.

WB₃ target absorption coefficient α and reflectivity R were $1.7 \times 10^5 \text{ m}^{-1}$ and 0.55 for 355 nm laser wavelength and $1.0 \times 10^5 \text{ m}^{-1}$ and 0.73 for 1064 nm laser wavelength, respectively [30]. The absorption and emission coefficients of plasma were described in [25].

For the plasma, the calculation domain was $r = 0.01 \text{ m}$ and $z = 0.025 \text{ m}$ with nonuniform grid with 60×200 nodes. The smallest computational cells had dimensions of $50 \times 0.1 \mu\text{m}$ at the vapour inlet. In the case of the target, the calculation domain was $r = 0.005 \text{ m}$ and $z = 2 \times 10^{-6} \text{ m}$ with 130×500 nodes, respectively. While the smallest computational cells had dimensions of $12 \times 0.004 \mu\text{m}$ at the target surface, the cell dimensions were fit to appearing gradients after preliminary calculations. Next, it was checked that further decreasing of cell dimensions did not change the results. The time step was adjusted to the smallest cells. Both cases were time-dependent and were solved in axisymmetric geometry. In the case of the plasma, the system of equations was solved by density-based (coupled) solver [24] with second-order spatial discretization for flow. The default settings [24] were applied for the target.

4. Results and Discussion

4.1. Mechanisms of Ablation. During the interaction of the laser beam with a material, the target is heated to a temperature exceeding its boiling point and sometimes its critical temperature [11, 13]. Assuming a constant fluence, the different mechanisms of ablation can occur depending on the critical temperature. In the case where the target temperature is lower than $0.9T_c$, mainly evaporation occurs. Explosive boiling begins above this limit. This phenomenon results in nanoparticles and microparticles with target composition present in the plasma plume, besides the expected electrons, ions, and neutrals. Both models can be observed during the ablation of tungsten and boron, depending on the laser fluence. Due to the high critical temperature (14778 K [31]) and high absorption coefficients 4.4×10^7 (reflectivity $R_{1064} = 60\%$) and $8.9 \times 10^7 \text{ 1/m}$ (reflectivity $R_{355} = 47\%$) [32], respectively, for 1064 nm and 355 nm laser wavelengths, tungsten is a material for which evaporation takes place primarily for the laser intensity below $6 \times 10^{10} \text{ W/cm}^2$ [33]. Figure 1 shows evolution of surface temperature at beam centre $r = 0$ for laser wavelengths 1064 nm and 355 nm for tungsten and boron at the laser fluence 10 J/cm^2 . For tungsten and the first harmonic of an Nd:YAG laser, the maximum surface temperature is 11700 K and for the third 13700 K (Figure 1(a)). In both cases, the maximum surface temperature is reached in 16 ns. At the next time steps, the temperature suddenly decreases due to absorption of the laser beam in the plasma.

The laser ablation mechanism is different in the case of boron. For both laser harmonics, the maximum temperatures exceed the critical temperature (Figure 1(b)), which is about 10000 K [31]. In this case, the explosive boiling occurs, which results in a film on which there are different sized irregularly shaped contaminants (Figures 2(a) and 2(b)).

The number and size of debris depend mainly on the optical properties of boron. In the case of $\lambda = 1064 \text{ nm}$,

the absorption coefficient is $1.3 \times 10^6 \text{ m}^{-1}$ (reflectivity $R_{1064} = 28.7\%$) [34] and is 23 times lower than for 355 nm (reflectivity $R_{355} = 28.6\%$). The low absorption coefficient results in a much thicker layer of heated material and the critical temperature is exceeded much further (Figure 3).

The result is an increase in the amount of larger fragments of the target in the deposited film. The maximum temperature for 1064 nm is obtained only in 22 ns. Due to the small amount of vaporized material, there is practically no plasma absorption. The high maximum temperature $\sim 19000 \text{ K}$ is the result of failure of the model neglecting phenomenon of explosive boiling. The rate of temperature equalization with increasing of distance over time is controlled by the coefficient of thermal diffusivity $a = k/(\rho c_p)$. Above the melting point, where it is assumed that the thermal properties and the density do not change, the value of diffusion coefficient is 2.58×10^{-5} and $1.48 \times 10^{-6} \text{ m}^2/\text{s}$ for tungsten and boron, respectively. The magnitude of this parameter indicates that subsurface overheating of a boron target is equalized much more slowly than in the case of tungsten. Moreover, in the case of tungsten, in connection with larger absorption coefficients, the laser beam penetrates the target to a lower depth. Both of these phenomena result in the maximum temperature located at the surface and the ablation process mainly by the evaporation of the surface. As a result, the surface of deposited tungsten films is smooth (Figures 2(c) and 2(d)).

This phenomenon is quite different in the case of boron when evaporation from the surface results in maximum of temperature placed at a certain depth. The critical temperature is achieved earlier below surface. The target surface erupts as a result of high stress. In the case of 1064 nm, a large amount of energy is accumulated at a depth of about $1 \mu\text{m}$. Lower thermal diffusivity of boron causes the increase of target cooling time (Figure 1(b)). The studies of ablation of nonmetallic materials showed that the process should be carried out with a sufficiently low fluence in order to avoid the phase explosion [11, 13]. However, in the case of boron ablation with the first harmonic, such a procedure could result in temperature decrease below the critical but simultaneously could cause the lack of ablation. The comparison of calculated and experimental tungsten crater (made with 355 nm radiation) is presented in Figure 4. The sample crater was formed by 50 laser shots in tungsten target.

The calculated depth of crater for one pulse was determined on the base of Hertz-Knudsen equation [13] described the rate of evaporation $\rho \cdot u$, which was integrated over time and radius. The calculated depth of the crater is 75.8 nm per pulse and is in good agreement with the experimentally measured values in our laboratory and by Spiro et al. [35] ($63 \pm 9 \text{ nm/pulse}$). Both experiments were conducted in similar conditions as were implemented in theoretical model. The cross section of crater in boron target ablated with 1064 nm wavelength after 50 laser pulses is presented in Figure 5. The depth of the crater is about $3 \mu\text{m}$ per pulse and is much deeper than the distance from surface where critical temperature is achieved (Figure 3). Formation of deep craters during ablation of boron could not be explained by the evaporation and explosive boiling alone.

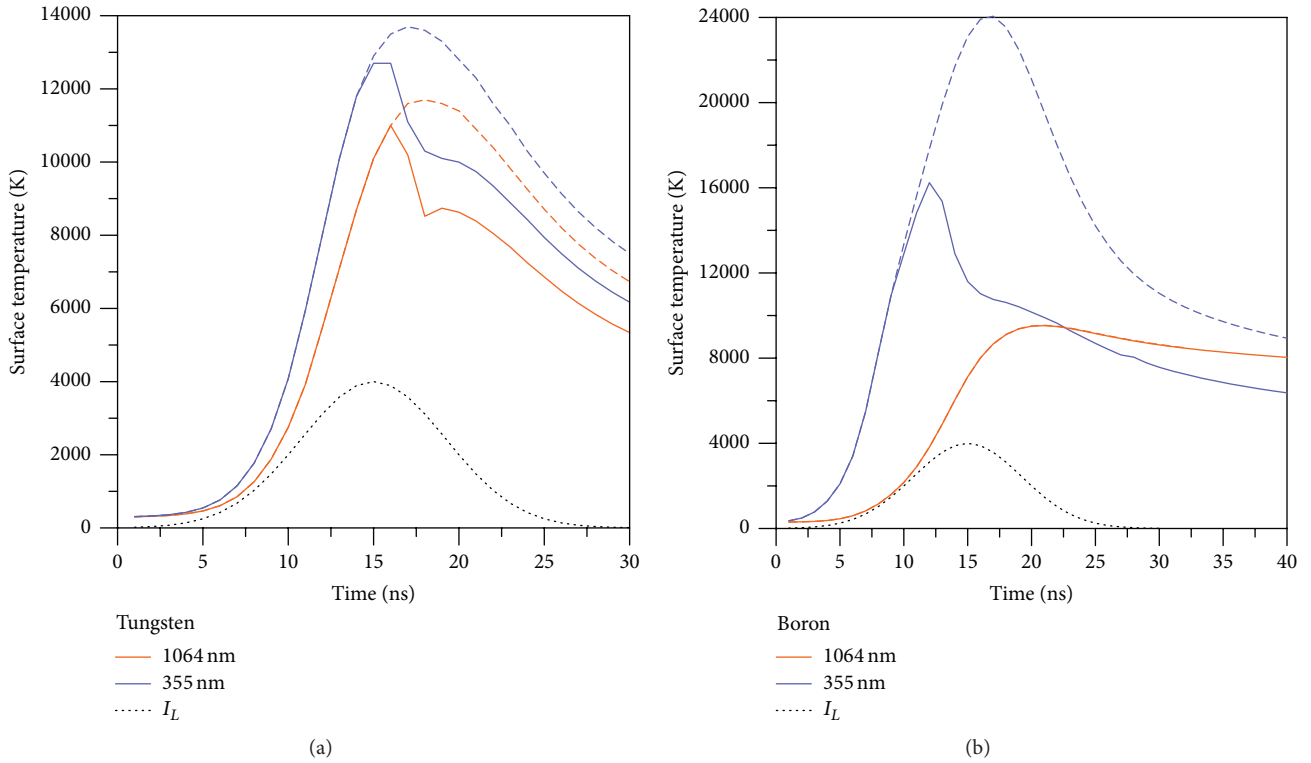


FIGURE 1: Target surface temperature T_s and laser intensity I_L during first 40 ns ($r = 0$). (a) Tungsten target and (b) boron target. Broken line denotes case without plasma absorption.

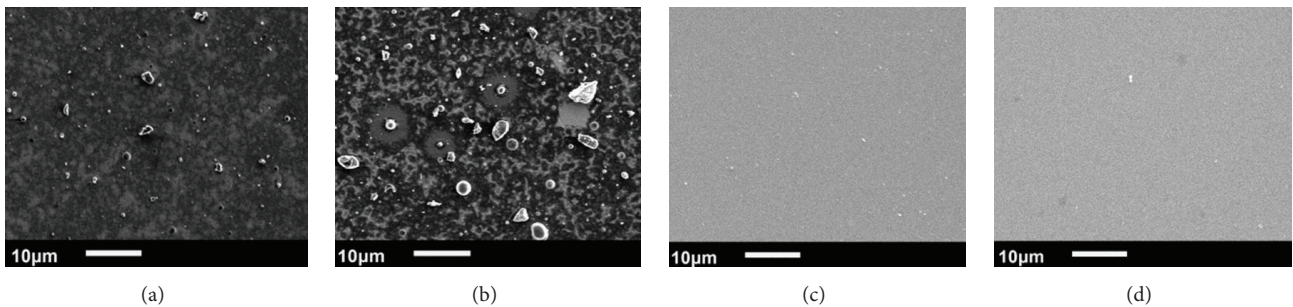


FIGURE 2: SEM micrograph ($\times 1000$) of deposited films: (a) boron 355 nm, (b) boron 1064 nm (c) tungsten 1064 nm, and (d) tungsten 355 nm. $F = 10 \text{ J/cm}^2$.

Existing models should be complemented with additional mass removal process. Experimental evidence suggests that this may be the mechanical forces arising as a result of the recoil pressure [36]. As suggested in [36], the recoil pressure at the surface of the target generates compression wave propagating deep into material. It has been shown that the longitudinal compression wave can cause fragmentation. Taking into account the depth and irregular profile of crater and shape and dimension of debris deposited on the target surface, it is very possible mechanism of ablation. The presented model in [36] is novel and should be checked for different materials in the future. In the case of boron, it is not possible currently because of lack of material parameters necessary for calculations.

4.2. Effect of the Ablation of Boron on the Deposition of WB_3 Films. As it is shown in Section 4.1, after exceeding of some threshold fluence, ablation of boron has an explosive character. This has an impact on the ablation process of composites containing boron such as WB_2/B . Figure 6(a) shows the WB_3 film deposited by PLD method from SPS sintered WB_2/B target [5]. Experiments were made for 355 nm wavelengths of an Nd:YAG laser and fluence $\sim 6 \text{ J} \times \text{cm}^{-2}$. The WB_3 thin films were deposited on a silicon substrate (SPI Supplies) at temperature of 600°C in vacuum ($2 \times 10^{-4} \text{ Pa}$) [5].

Deposited layer mainly consists of droplets of different sizes. The abundances of elements (from three independent spots) in the deposited film are $77.6 \pm 0.3\%$ tungsten, $21.8 \pm 0.3\%$ boron, and $0.49 \pm 0.04\%$ oxygen (percentages by weight),

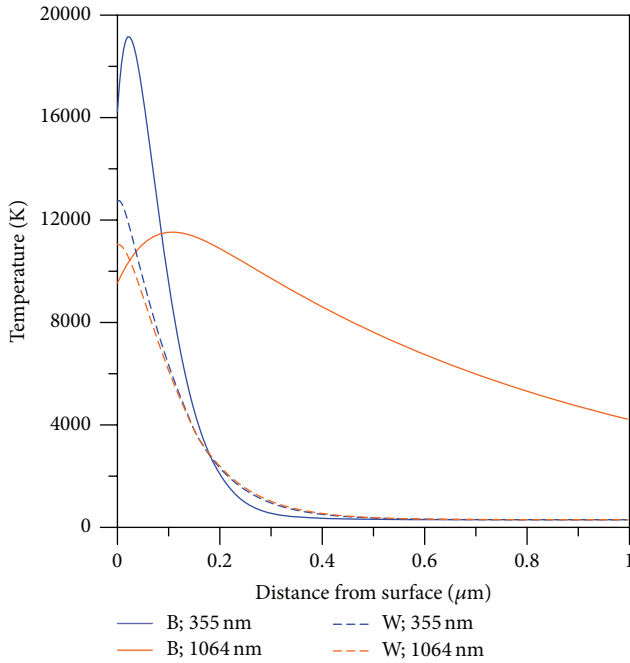


FIGURE 3: Target temperature T and laser intensity I_L along target axis at the time moments when the surface temperature reaches its maximum value.

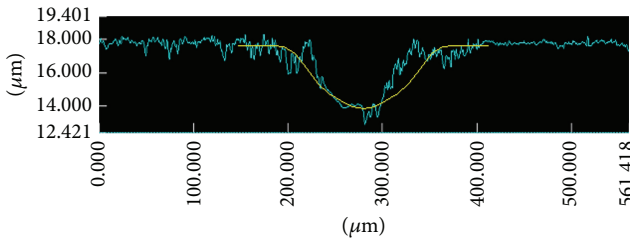


FIGURE 4: The cross section of crater from experiment (blue line) and theoretical calculation (yellow line). Target: tungsten; laser wavelength 355 nm; fluence 10 J/cm^2 ; 50 laser pulses.

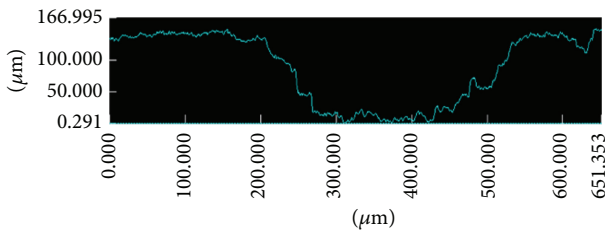


FIGURE 5: The cross section of crater in boron target ablated with 1064 nm wavelength after 50 laser pulses.

Figure 6(c). The B/W ratio found in deposited films is about 4.8, which is very close to the starting material ratio of 4.5 in target. The apparent differences may result from the peak of carbon which overlaps the peak of boron in the vicinity of 0.25 keV (Figure 6(b)). If the contribution of the advantageous carbon peak will be subtracted from the boron peak, the ratio arrived at may actually even be exactly 4.5.

The composition of deposited film is close to the target one. It indicates that film may be deposited mainly from melted debris of target but not due to condensation in plasma plume. Moreover, the high saturation ratios and presence of ionization lead to extraordinarily high nucleation rates and small critical radii. In the case of condensation, only clusters in the range of 5–50 nm can be produced [6, 7], which is above one hundred times less than dimension of droplets deposited in WB_3 films [5].

The creating of layers as a result of the deposition of droplets only is not a standard feature of the PLD and should be discussed. In Figure 7(a), SEM image of the WB_2/B target surface after ablation is presented. It shows the melted surface with a lot of holes.

The origin of holes can be correlated with the structure of the target presented in Figure 7(b). The dark areas mainly consist of pure boron [5]. Boron surface heats up much faster than the WB_2 surface. This is due to the higher reflectivity of laser radiation and a higher rate of temperature equalization for WB_2 . In the case of tungsten borides, these values are $R_{355} = 55\%$ and $a = 6.82 \times 10^{-6} \text{ m}^2/\text{s}$, respectively, while, for boron, 28.5% and $1.48 \times 10^{-6} \text{ m}^2/\text{s}$, respectively. Due to faster heating of boron, when it evaporates and then achieves critical temperature, the rest of material is melted only. This thesis is confirmed by temperature distributions on target axis for WB_2 and B, respectively (Figure 8). In the case of ablation of boron using 355 nm already at 9th nanosecond of pulse duration, the critical temperature ($\sim 10000 \text{ K}$) is achieved. At the same time, in the case of the target of pure WB_2 , the maximum temperature does not exceed 4000 K. Taking into account melting temperature of WB_2 (2833 K [26]), the maximum depth of the liquid phase reaches about $0.07 \mu\text{m}$ at 9th ns (Figures 8 and 9) and increases during next time steps to $0.6 \mu\text{m}$. After the cessation of laser impulse, the thermal diffusion and subsequent explosive boiling are a potential mechanism of droplets formation [14, 15]. The superheated liquid will undergo a transition into a mixture of vapour and liquid droplets, followed by delayed explosive boiling of the liquid-vapour mix.

Because of lack of appropriate WB_2 material properties, it is impossible to calculate the critical radius and the time for a spherically symmetric bubble in a superheated liquid volume [15]. However, as can be seen in Figure 9, after 100 ns, depth of melted material does not exceed $0.6 \mu\text{m}$. At the same time, the maximum temperature falls below the boiling point of the both components of WB_2/B . This excludes the possibility of delayed explosive boiling and ejecting droplets with size of a few microns. It should be noted that the calculated depth of melting is in a satisfactory accord with the experimental results [5].

Therefore, the explosive release of the boron and related “detonation in liquid phase” can explain the large droplets found on the substrate. During laser heating, the pressure in boron is growing. Due to Hertz-Knudsen equation [13], the achieved vapour pressure is about $3 \times 10^8 \text{ Pa}$ when temperature is close to the critical. Abrupt grow of temperature and pressure causes creation of the detonation waves [37, 38]. Next, propagating shocks cause compression

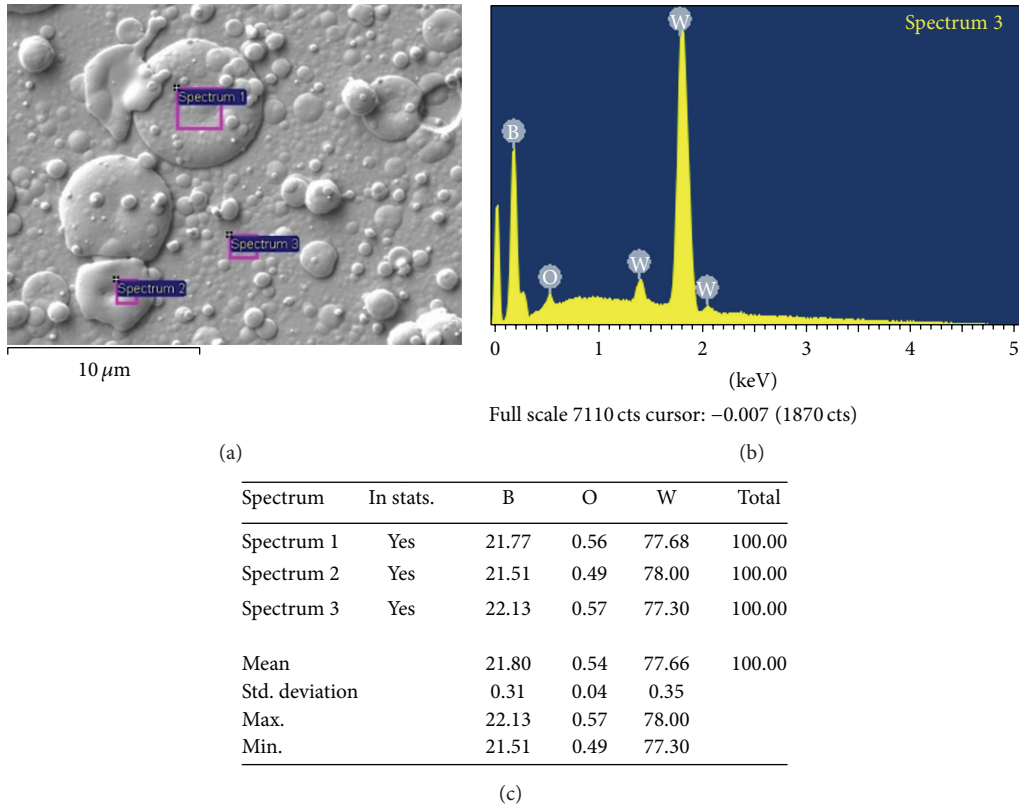


FIGURE 6: SEM micrograph of deposited WB_3 film (magnification $\times 5000$) with EDS measurement points (a) and the abundances of elements in the deposited film in the spot spectrum 3 (b) and table reporting the composition of the film in examined areas (c).

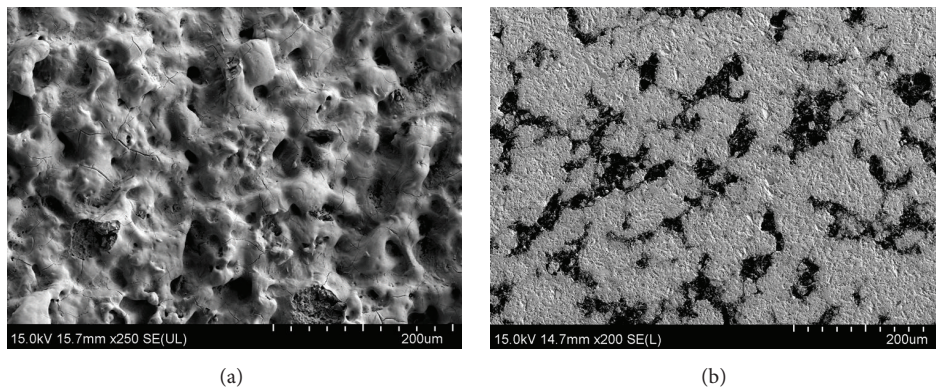


FIGURE 7: SEM microphotographs: (a) ablated target surface and (b) cross section of not yet ablated target [5].

of liquid WB_2 . When the pressure between two or more waves is large enough to balance the forces associated with surface tension of WB_2 , the ejection of droplets occurs. At the places where the distance between boron islands is too high (Figure 7(b)), the evaporation [22], fragmentation [36], and boiling explosion [15, 36] are possible mechanisms of ablation. The comparison of ablation mechanisms is schematically depicted in Figure 10. It should be noted that in all cases ablation parameters are the same changing only material of target.

During the interaction of the laser beam with a material, the target is heated to a temperature exceeding its boiling point. Evaporation takes place when the pressure ratio p_{KL}/p_{sat} across the Knudsen layer KL is lower than unity, where p_{KL} denotes pressure on the end of KL and p_{sat} —saturation pressure. Material evaporated from the target forms a thin layer of dense plume, consisting of electrons, ions, and neutrals (Figure 10(a)). It is assumed that the explosive boiling begins when the target temperature exceeds 0.9 of the critical temperature (Figure 10(b)). This type of

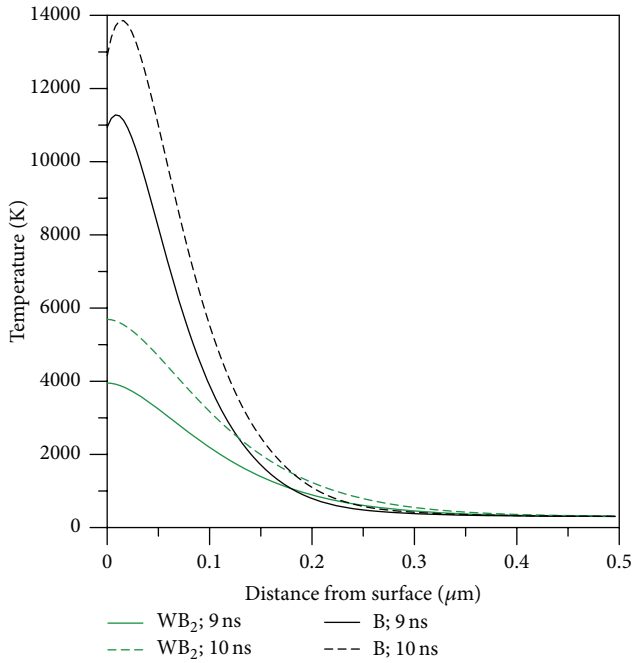


FIGURE 8: Distribution of target temperature along the axis at 9th ns and 10th ns from the beginning of laser pulse. Targets material: WB_2 and B; laser radiation 355 nm.

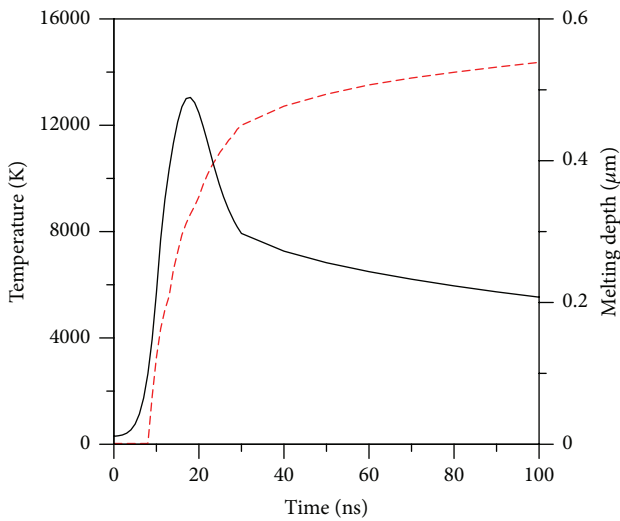


FIGURE 9: Target maximum temperature and melting depth during first 100 nanoseconds ($r = 0$). Broken line denotes melting depth of WB_2 target.

ablation results in the appearance of superheated particles in the plasma plume. In Figure 10(c) described above, “detonation in liquid phase” is shown. Due to such mechanisms of ablation, it is evident that the main constituent of the deposited film is large number of droplets from detonation. However, the smaller droplets can also be formed by gas phase condensation [39]. The overall morphology does not change with laser fluence ($2.5\text{--}10\text{ J/cm}^2$) and studied laser wavelength.

It should be noted that described mechanism of ablation is a special case related to the specific target and cannot be generalized, but it is possible in targets with boron excess.

XRD studies and nanoindentation of deposited layer show the additional effect occurring during laser ablation target WB_2/B . The effect is a phase change from WB_2/B to WB_3 [5]. It occurs most likely due to a very large gradients of temperature and pressure in the target and subsequently in the plasma.

4.3. Plasma. The temperature and velocity of plasma are responsible for the deposition rate of the film and its adhesion. Also, the shielding effects due to the absorption and radiation of plasma may have an impact on the course of ablation. All these parameters are dependent on laser wavelengths. The calculated distributions of plasma temperature and density after 100 ns of expansion (Figure 11) show that plasma temperatures are higher in the case of 1064 nm, but the densities and pressures are higher in the case of 355 nm, which is in agreement with experimental findings [40]. Smaller penetration depth and reflection coefficient R in the case of 355 nm causes a higher surface temperature of the target and thus a greater rate of ablation. The greater ablation rate results in larger mass density of the ablated plume and, hence, in higher pressures. An additional consequence of a higher ablation rate is slower expansion and smaller dimensions of the plasma plume. Higher plasma temperature in the case of 1064 nm is the result of lower density and stronger plasma absorption. At 100 ns after the beginning of the laser pulse, the maximum temperature for the third harmonic is 2 times lower than in the case of the first harmonic of laser irradiation and is about 45000 K. The decrease in density due to the expansion and intensive absorption of energy from the laser beam causes a rapid increase of temperature and velocity. After 100 ns, the velocity of the plume ablated by 355 nm is 14850 m/s, while the velocity of the plume ablated by 1064 nm reaches 20750 m/s.

For comparison, the plasma plume propagation was studied by optical imaging at 80–400 ns time delay after the laser shot. The images of tungsten plasma at delay time 100, 200, 300, 400 ns for 355 nm and 1064 nm are presented in Figures 12(a) and 12(b), respectively.

For every single image of the plasma plume, the half-Lorentzian plot was fitted to an axis intensity. For comparison, Figures 12(c) and 12(d) show ICCD images of boron and WB_2/B plasma formed during ablation with a wavelength of 355 nm. The boron plasma plume is much larger than tungsten plume and moves at the speed of 44×10^3 m/s, which is consistent with the results presented in [22]. In the case of WB_2/B plasma, the total velocity is similar to tungsten plasma (18500 m/s). It is worth noting that, contrary to the plumes of pure boron and pure tungsten which move with different velocities (Figures 12(a) and 12(c)) in WB_2/B plasma, both components are mixed and move with approximately the same velocity.

The Lorentzian plot position is taken as a maximum intensity of the plasma plume, and FWHM is a level of plasma expansion.

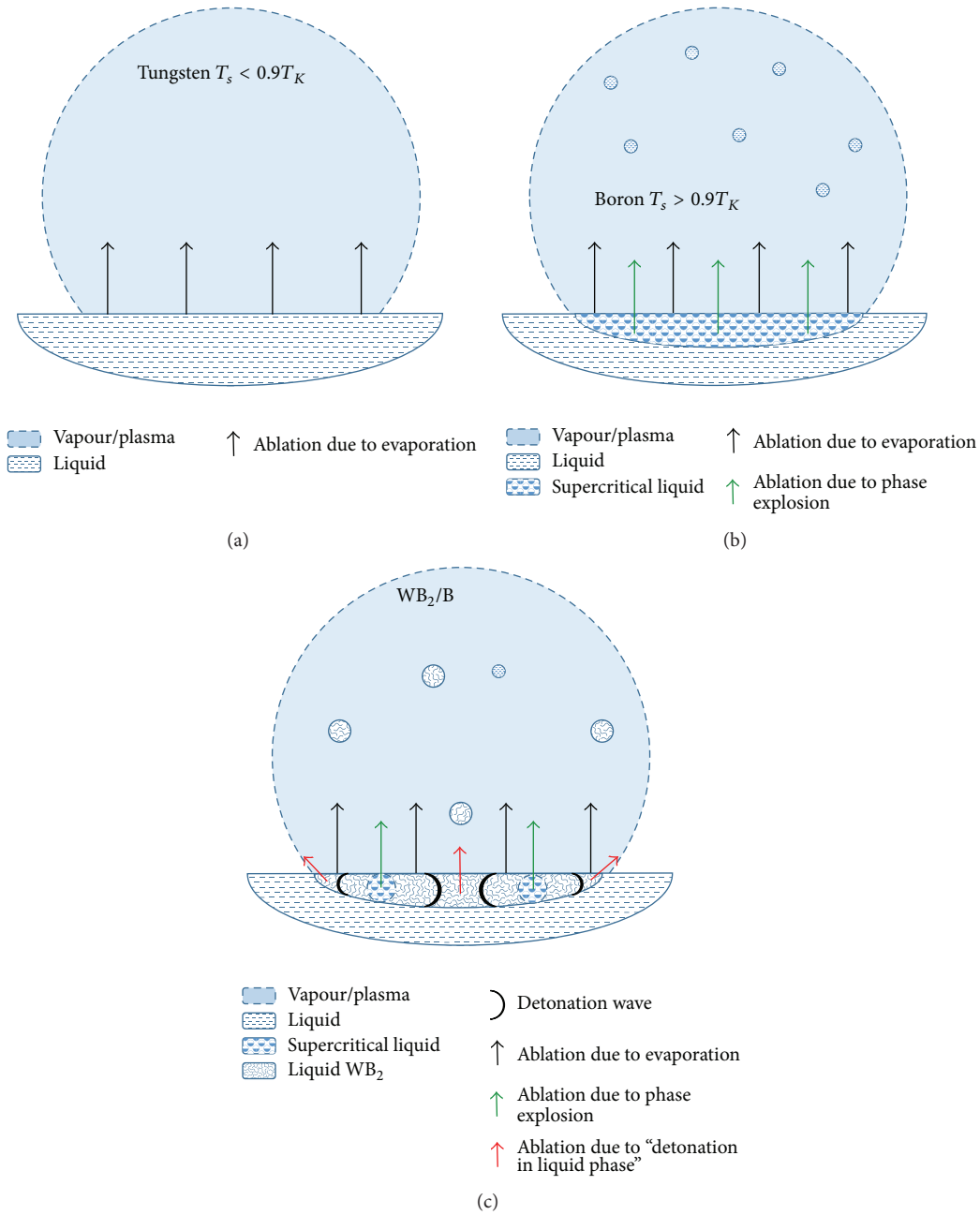


FIGURE 10: The comparison of ablation mechanisms: (a) evaporation, (b) phase explosion, and (c) "detonation in liquid phase."

Figure 13 presents tungsten plasma position and FWHM of Lorentzian plot fitted to plasma intensity distribution. On the basis of plasma propagation and expansion in time, the plasma displacement and expansion velocity were calculated, respectively. Total velocity of plasma front is defined as a sum of both velocities mentioned above. Results are presented in Table 1.

The quantitative comparison of the experimental plasma shape with the theoretical results is difficult because the images show plasma radiation, which depends both on plasma density and temperature. However, plasma dimensions

are similar; for example, after 100 ns, the tungsten plasma diameter is about 2 mm. The front velocities obtained from the experimental plasma images are only 10% lower than those calculated in the model. For comparison, Figure 12(c) shows the sequence of ICCD images of boron plasma formed during ablation with a wavelength of 355 nm. The boron plasma plume is much larger than tungsten plume and moves at the speed of 44×10^3 m/s, which is consistent with the results presented in [22].

For the fluence 10 J/cm^2 , the total absorption of the laser beam in the plasma plume is 6% in the case of 355 nm

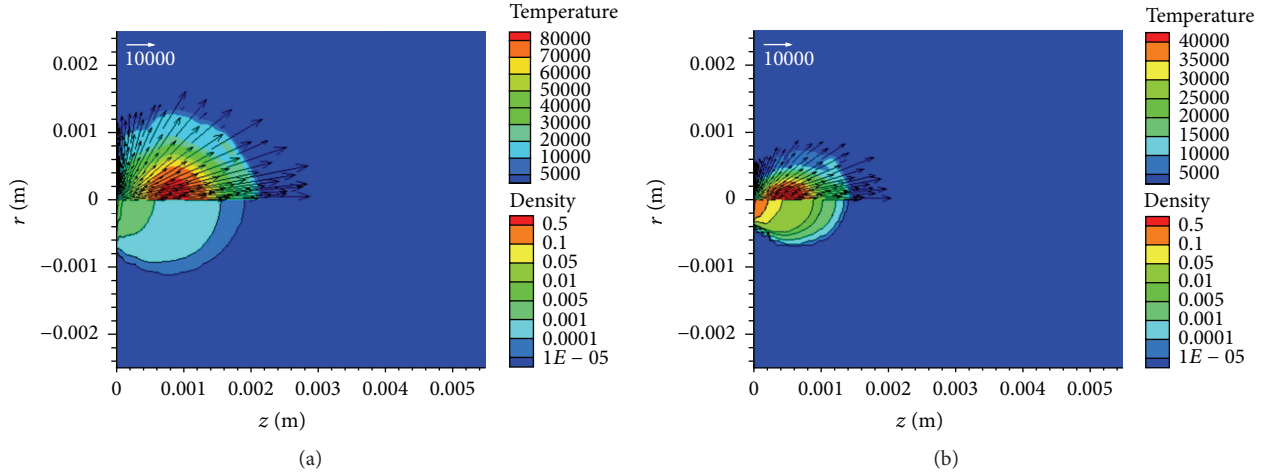


FIGURE 11: Distribution of density, temperature, and velocity in plasma induced during laser ablation of tungsten 100 ns after the beginning of the laser pulse for (a) 1064 nm and (b) 355 nm laser wavelength.

TABLE 1: Comparison of tungsten plasma velocity of W, B, and WB_2/B .

	Tungsten 355 nm	Tungsten 1064 nm	Boron 355 nm	WB_2/B 355 nm
Plasma displacement [m/s]	3580	5800	9305	8300
Plasma expansion [m/s]	10545	13000	32715	10200
Total velocity [m/s]	14125	18800	42017	18500
Model	14850	20750	~44000 [22]	—

radiation and about 3.5% in the case of 1064 nm. In this case, due to the small amount of absorbed energy, the plasma radiation does not affect the target heating.

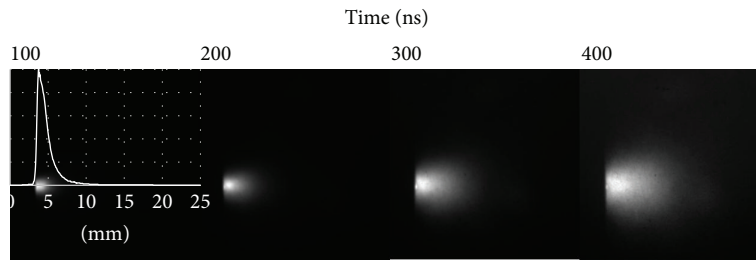
5. Summary

In this paper, the interaction of Nd:YAG nanoseconds laser beam with WB_2/B , tungsten, and boron target induced during ablation plasma was studied. The investigations for two wavelengths of an Nd:YAG laser—355 nm and 1064 nm—and fluence of 10 J/cm^2 were made. On the base of results from the theoretical model and experimental investigations, the conclusions are as follows:

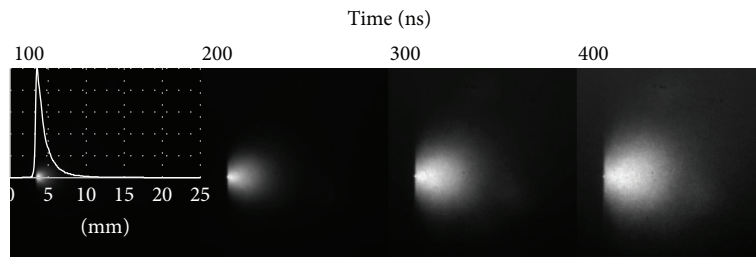
- (1) The studies show the fundamental differences in ablation of WB_2/B , tungsten, and boron targets used for deposition of WB_3 superhard films. In case of tungsten, the evaporation of material is controlled by the plasma formation and consequently the absorption coefficient. The dense plasma plume can block laser radiation and limit energy transfer from the laser beam to the material. For boron, the explosive ablation is observed. Such behaviour is affected by

subsurface heating and transition to supercritical state. In the case of 1064 nm wavelength, the effect is magnified by the high penetration depth of the laser beam. Explosive nature of the ablation of boron has a crucial influence on the ablation of WB_2/B composite. The faster heating of boron in comparison with WB_2 case that, at the moment, when the boron exceeds a critical temperature, the rest of material is melted only. The laser beam causes the faster heating of boron than tungsten diboride. As a result, boron exceeds a critical temperature, when the rest of material is melted only. It results in the explosion in liquid phase and deposition of WB_3 film mainly from droplets embedded in continuous matrix. The creating of layers as a result of the deposition mainly from droplets is not a standard feature of the PLD. Therefore, in ceramics target with a boron excess [1, 5, 41], there may be adverse phenomena which have impact on the quality of the deposited film.

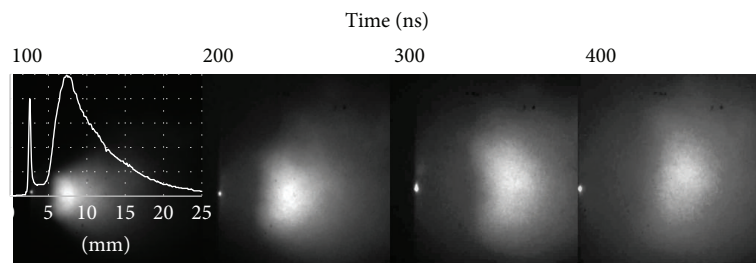
- (2) In the case of boron ablation with the laser wavelength 1064 nm, the main reason of the higher amount of debris on the surface of the deposited films is the low absorption coefficient ($1.3 \times 10^6 \text{ m}^{-1}$). It causes the heating of much more material and the critical temperature is exceeded much later and at a greater depth than for 355 nm. It should be noted that, in so far described cases [21], the use of 1064 nm wavelength results in the deposition of films significantly smoother than 355 nm at the same fluence.
- (3) Using of shorter wavelength (355 nm here) with the higher absorption coefficient causes faster heating of the target and thus higher ablation rate.
- (4) A method estimating phase explosion occurrence based on material data such as critical temperature, thermal diffusivity, and optical properties is shown.



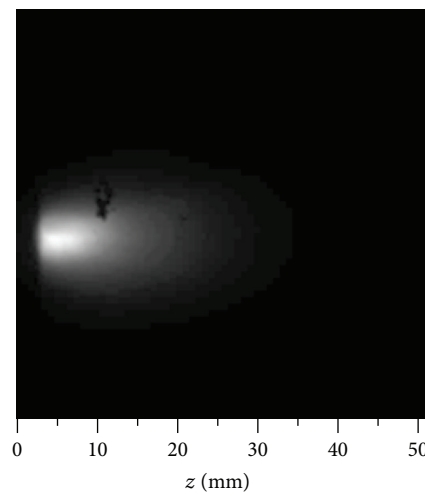
(a)



(b)



(c)



(d)

FIGURE 12: ICCD images of tungsten plasma for (a) tungsten 355 nm, (b) tungsten 1064 nm, (c) boron 355 nm, and (d) WB_2/B 355 nm. Visible light, exposure time 20 ns, and delay time 100, 200, 300, 400 ns, respectively (WB_2/B after 400 ns). Solid line denotes the intensity distribution of plasma radiation on the axis of plasma $r = 0$.

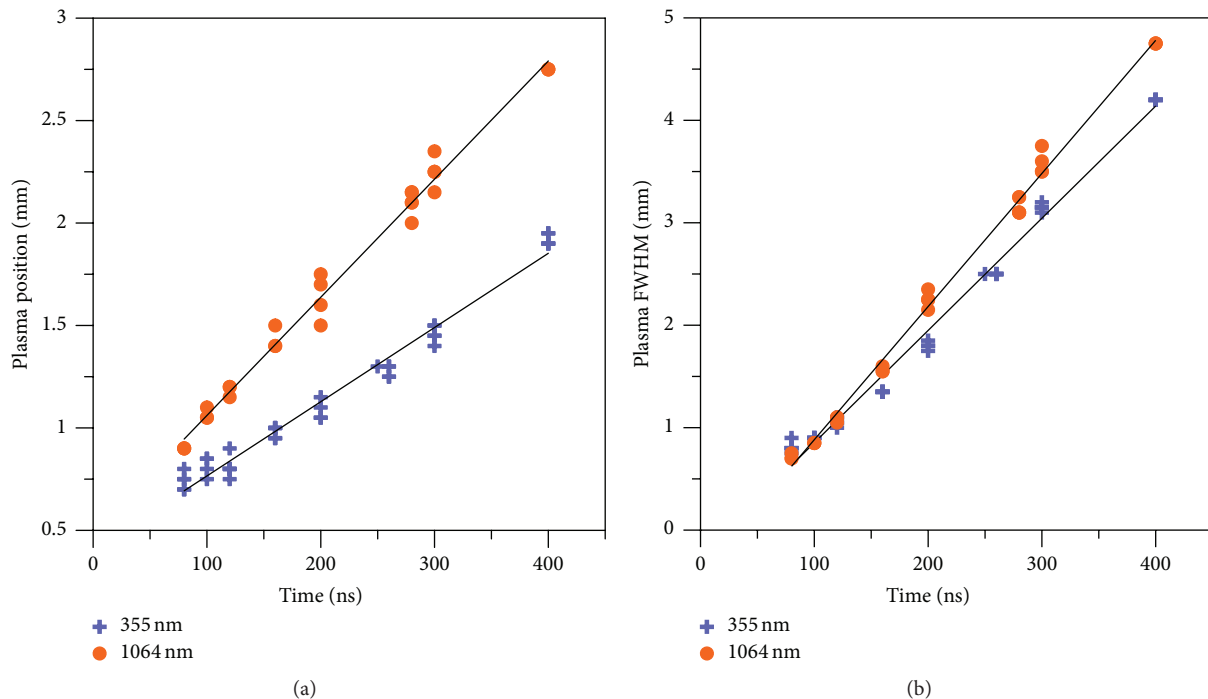


FIGURE 13: Experimental tungsten plasma plume parameters for 1064 and 355 nm laser wavelengths. (a) Velocity of plasma propagation and (b) velocity of plasma expansion.

Additional Points

- (1) The genesis of droplets in novel, superhard WB_3 films on the base of optical and material properties is explained.
- (2) The influence of laser wavelength on PLA/PLD of tungsten and boron is studied.
- (3) The new mechanism of ablation “detonation in liquid phase” is proposed.

Competing Interests

The author declares that there are no competing interests regarding the publication of this paper.

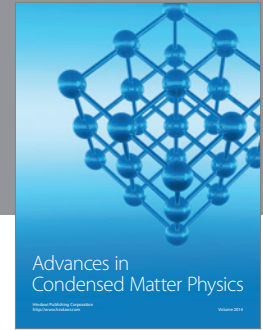
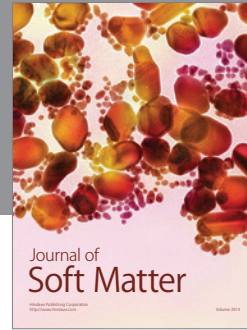
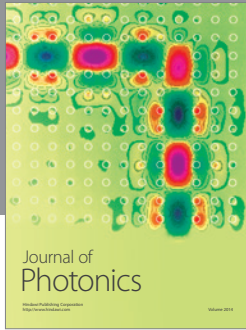
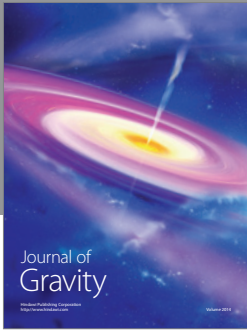
Acknowledgments

This work was supported by the National Science Centre (Poland) and Research Project: UMO-2012/05/D/ST8/03052. The author wishes to thank Dr. Jacek Hoffman and M.S. Justyna Chrzanowska for substantive discussion, suggestions, and help in experiment.

References

- [1] R. Mohammadi, A. T. Lech, M. Xie et al., “Tungsten tetraboride, an inexpensive superhard material,” *Proceedings of the National Academy of Sciences of the United States of America*, vol. 108, no. 27, pp. 10958–10962, 2011.
- [2] Y. Liang, Z. Fu, X. Yuan, S. Wang, Z. Zhong, and W. Zhang, “An unexpected softening from WB_3 to WB_4 ,” *Europhysics Letters*, vol. 98, no. 6, Article ID 66004, 2012.
- [3] J. V. Rau, A. Latini, R. Teghil et al., “Superhard tungsten tetraboride films prepared by pulsed laser deposition method,” *ACS Applied Materials and Interfaces*, vol. 3, no. 9, pp. 3738–3743, 2011.
- [4] D. Dellasega, G. Merlo, C. Conti, C. E. Bottani, and M. Passoni, “Nanostructured and amorphous-like tungsten films grown by pulsed laser deposition,” *Journal of Applied Physics*, vol. 112, no. 8, Article ID 084328, 2012.
- [5] T. Moscicki, J. Radziejewska, J. Hoffman et al., “ WB_2 to WB_3 phase change during reactive spark plasma sintering and pulsed laser ablation/deposition processes,” *Ceramics International*, vol. 41, no. 7, pp. 8273–8281, 2015.
- [6] T. Scholza and K. Dickmann, “Investigation on particle formation during laser ablation process with high brilliant radiation,” *Physics Procedia*, vol. 5, pp. 311–316, 2010.
- [7] M. S. Tillack, D. W. Blair, and S. S. Harilal, “The effect of ionization on cluster formation in laser ablation plumes,” *Nanotechnology*, vol. 15, no. 3, pp. 390–403, 2004.
- [8] Y. Cheng, M. Shigeta, S. Choi, and T. Watanabe, “Formation mechanism of titanium boride nanoparticles by RF induction thermal plasma,” *Chemical Engineering Journal*, vol. 183, pp. 483–491, 2012.
- [9] L. D’Alessio, D. Ferro, V. Marotta, A. Santagata, R. Teghil, and M. Zaccagnino, “Laser ablation and deposition of Bioglass® 45S5 thin films,” *Applied Surface Science*, vol. 183, no. 1-2, pp. 10–17, 2001.
- [10] R. K. Singh and J. Narayan, “Pulsed-laser evaporation technique for deposition of thin films: physics and theoretical model,” *Physical Review B*, vol. 41, no. 13, pp. 8843–8859, 1990.

- [11] R. Kelly and A. Miotello, "Comments on explosive mechanisms of laser sputtering," *Applied Surface Science*, vol. 96–98, pp. 205–215, 1996.
- [12] N. M. Bulgakova, A. B. Evtushenko, Y. G. Shukhov, S. I. Kudryashov, and A. V. Bulgakov, "Role of laser-induced plasma in ultradeep drilling of materials by nanosecond laser pulses," *Applied Surface Science*, vol. 257, no. 24, pp. 10876–10882, 2011.
- [13] N. M. Bulgakova and A. V. Bulgakov, "Pulsed laser ablation of solids: transition from normal vaporization to phase explosion," *Applied Physics A: Materials Science and Processing*, vol. 73, no. 2, pp. 199–208, 2001.
- [14] Q. Lu, S. S. Mao, X. Mao, and R. E. Russo, "Delayed phase explosion during high-power nanosecond laser ablation of silicon," *Applied Physics Letters*, vol. 80, no. 17, pp. 3072–3074, 2002.
- [15] J. H. Yoo, S. H. Jeong, X. L. Mao, R. Greif, and R. E. Russo, "Evidence for phase-explosion and generation of large particles during high power nanosecond laser ablation of silicon," *Applied Physics Letters*, vol. 76, no. 6, pp. 783–785, 2000.
- [16] T. A. Friedmann, K. F. McCarty, E. J. Klaus et al., "Pulsed laser deposition of BN onto silicon (100) substrates at 600°C," *Thin Solid Films*, vol. 237, pp. 48–56, 1994.
- [17] N. M. Bulgakova, V. P. Zhukov, A. R. Collins, D. Rostohar, T. J.-Y. Derrien, and T. Mocek, "How to optimize ultrashort pulse laser interaction with glass surfaces in cutting regimes?" *Applied Surface Science*, vol. 336, pp. 364–374, 2015.
- [18] M. Afif, J. P. Girardeau-Montaut, C. Tomas et al., "In situ surface cleaning of pure and implanted tungsten photocathodes by pulsed laser irradiation," *Applied Surface Science*, vol. 96–98, pp. 469–473, 1996.
- [19] J.-W. Yoon and K. B. Shim, "Growth of crystalline boron nanowires by pulsed laser ablation," *Journal of Ceramic Processing Research*, vol. 12, no. 2, pp. 199–201, 2011.
- [20] A. Suslova, O. El-Atwani, S. S. Harilal, and A. Hassanein, "Material ejection and surface morphology changes during transient heat loading of tungsten as plasma-facing component in fusion devices," *Nuclear Fusion*, vol. 55, no. 3, Article ID 033007, 2015.
- [21] Q. Lu, S. S. Mao, X. Mao, and R. E. Russo, "Theory analysis of wavelength dependence of laser-induced phase explosion of silicon," *Journal of Applied Physics*, vol. 104, no. 8, Article ID 083301, 2008.
- [22] T. Moscicki, "Expansion of laser-ablated two-component plume with disparate masses," *Physica Scripta T*, vol. 161, Article ID 014024, 2014.
- [23] J. Hoffman, T. Moscicki, and Z. Szymanski, "Acceleration and distribution of laser-ablated carbon ions near the target surface," *Journal of Physics D: Applied Physics*, vol. 45, no. 2, Article ID 025201, 2012.
- [24] ANSYS, ANSYS® *Academic Research, Release 16.0, Help System, Fluent Documentation*, ANSYS, Canonsburg, Pa, USA, 2015.
- [25] T. Moscicki, J. Hoffman, and J. Chrzanowska, "The absorption and radiation of a tungsten plasma plume during nanosecond laser ablation," *Physics of Plasmas*, vol. 22, no. 10, Article ID 103303, 2015.
- [26] C. L. Jiang, Z. L. Pei, Y. M. Liu, H. Lei, J. Gong, and C. Sun, "Determination of the thermal properties of AlB_2 -type WB_2 ," *Applied Surface Science*, vol. 288, pp. 324–330, 2014.
- [27] M. S. Kovalchenko, L. G. Bodrova, V. F. Nemchenko, and V. F. Kolotun, "Some physical properties of the higher borides of molybdenum and tungsten," *Journal of the Less-Common Metals*, vol. 67, no. 2, pp. 357–362, 1979.
- [28] J. M. Leitnaker, M. G. Bowman, and P. W. Gilles, "High-temperature evaporation and thermodynamic properties of zirconium diboride," *The Journal of Chemical Physics*, vol. 36, no. 2, pp. 350–358, 1962.
- [29] A. S. Bolgar, T. S. Verkhoglyadova, and G. V. Samsonov, "Vapor pressure and evaporation rate of certain heat-resistant compounds in a vacuum at high temperatures," *Izvestiya Akademii Nauk SSSR, Otdeleniye Tekhnicheskikh Nauk, Metallurgiya i Toplivo*, vol. 1, pp. 142–145, 1961.
- [30] Y.-F. Wang, Q.-L. Xia, and Y. Yu, "First principles calculation on electronic structure, chemical bonding, elastic and optical properties of novel tungsten triboride," *Journal of Central South University*, vol. 21, no. 2, pp. 500–505, 2014.
- [31] S. Blairs and M. H. Abbasi, "Correlation between surface tension and critical temperatures of liquid metals," *Journal of Colloid and Interface Science*, vol. 304, no. 2, pp. 549–553, 2006.
- [32] A. D. Rakić, A. B. Djurišić, J. M. Elazar, and M. L. Majewski, "Optical properties of metallic films for vertical-cavity optoelectronic devices," *Applied Optics*, vol. 37, no. 22, pp. 5271–5283, 1998.
- [33] K. Yahiaoui, T. Kerdja, and S. Malek, "Phase explosion in tungsten target under interaction with Nd:YAG laser tripled in frequency," *Surface and Interface Analysis*, vol. 42, no. 6-7, pp. 1299–1302, 2010.
- [34] N. Morita and A. Yamamoto, "Optical and electrical properties of boron," *Japanese Journal of Applied Physics*, vol. 14, no. 6, article 825, 1975.
- [35] A. Spiro, M. Lowe, and G. Pasmanik, "Drilling rate of five metals with picosecond laser pulses at 355, 532, and 1064 nm," *Applied Physics A*, vol. 107, no. 4, pp. 801–808, 2012.
- [36] J. Hoffman, "The effect of recoil pressure in the ablation of polycrystalline graphite by a nanosecond laser pulse," *Journal of Physics D: Applied Physics*, vol. 48, no. 23, Article ID 235201, 2015.
- [37] Y. B. Zel'dovich, V. B. Librovich, G. M. Makhviladze, and G. I. Sivashinsky, "On the development of detonation in a non-uniformly preheated gas," *Astronautica Acta*, vol. 15, no. 5-6, pp. 313–321, 1970.
- [38] F. Zhang, Ed., *Shock Wave Science and Technology Reference Library, Volume 4: Heterogeneous Detonation*, Springer, 2009.
- [39] R. Teghil, L. D'Alessio, M. Zaccagnino, D. Ferro, V. Marotta, and G. De Maria, "TiC and TaC deposition by pulsed laser ablation: a comparative approach," *Applied Surface Science*, vol. 173, no. 3-4, pp. 233–241, 2001.
- [40] A. E. Hussein, P. K. Diwakar, S. S. Harilal, and A. Hassanein, "The role of laser wavelength on plasma generation and expansion of ablation plumes in air," *Journal of Applied Physics*, vol. 113, no. 14, Article ID 143305, 2013.
- [41] H. H. Itoh, T. Matsudaira, S. Naka, H. Hamamoto, and M. Obayashi, "Formation process of tungsten borides by solid state reaction between tungsten and amorphous boron," *Journal of Materials Science*, vol. 22, no. 8, pp. 2811–2815, 1987.



Hindawi

Submit your manuscripts at
<http://www.hindawi.com>

